

Article

Theoretical Exploration of Various Lithium Peroxide Crystal Structures in a Li-Air Battery

Kah Chun Lau ^{1,*}, Dantong Qiu ^{2,†}, Xiangyi Luo ², Jeffrey Greeley ³, Larry A. Curtiss ¹, Jun Lu ^{2,*} and Khalil Amine ²

¹ Materials Science Division, Argonne National Laboratory, 9700 South Cass Avenue, Argonne, IL 60439, USA; E-Mail: curtiss@anl.gov

² Chemical Sciences and Engineering Division, Argonne National Laboratory, 9700 South Cass Avenue, Argonne, IL 60439, USA; E-Mails: qiu950721@live.com (D.Q.); xy.luo@anl.gov (X.L.); amine@anl.gov (K.A.)

³ Purdue University, School of Chemical Engineering, Forney Hall of Chemical Engineering, 480 Stadium Mall Drive, West Lafayette, IN 47907-2100, USA; E-Mail: jgreeley@purdue.edu

† Current Address: Beijing Technology and Business University, Beijing 100048, China.

* Authors to whom correspondence should be addressed;
E-Mails: kclau@anl.gov (K.C.L.); junlu@anl.gov (J.L.);
Tel.: +1-630-252-3498 (K.C.L.); +1-630-252-4485 (J.L.);
Fax: +1-630-252-9555 (K.C.L.); +1-630-252-4176 (J.L.).

Academic Editor: Sheng S. Zhang

Received: 11 November 2014 / Accepted: 6 January 2015 / Published: 14 January 2015

Abstract: We describe a series of metastable Li₂O₂ crystal structures involving different orientations and displacements of the O₂²⁻ peroxy ions based on the known Li₂O₂ crystal structure. Within the vicinity of the chemical potential $\Delta G \sim 0.20$ eV/Li from the thermodynamic ground state of the Li₂O₂ crystal structure (*i.e.*, Föppl structure), all of these newly found metastable Li₂O₂ crystal structures are found to be insulating and high-*k* materials, and they have a common unique signature of an O₂²⁻ O-O vibration mode ($\omega \sim 799\text{--}865$ cm⁻¹), which is in the range of that commonly observed in Li-air battery experiments, regardless of the random O₂²⁻ orientations and the symmetry in the crystal lattice. From XRD patterns analysis, the commercially available Li₂O₂ powder is confirmed to be the thermodynamic ground state Föppl-like structure. However, for Li₂O₂ compounds that are grown electrochemically under the environment of Li-O₂ cells, we found that the XRD patterns alone are not sufficient for structural identification of these metastable Li₂O₂ crystalline phases due to the poor crystallinity

of the sample. In addition, the commonly known Raman signal of O_2^{2-} vibration mode is also found to be insufficient to validate the possible existence of these newly predicted Li_2O_2 crystal structures, as all of them similarly share the similar O_2^{2-} vibration mode. However considering that the discharge voltage in most Li- O_2 cells are typically several tenths of an eV below the thermodynamic equilibrium for the formation of ground state Föpl structure, the formation of these metastable Li_2O_2 crystal structures appears to be thermodynamically feasible.

Keywords: Li-air battery; lithium peroxide; crystal structure; DFT calculation

1. Introduction

Of particular interest in the context of future transportation needs for high energy density in energy storage, Li- O_2 (or Li-air) electrochemical cells are often touted as a potentially promising technological successor to current Li-ion batteries. Through directly reacting with the O_2 gas at the cathode, the reactions involving Li and O_2 are thermodynamically favorable and can potentially yield a high energy density and high specific energy [1–5]. Although many possible side reactions have been observed in Li-air cells when in operation [3–7], the fundamental reaction should ideally involve only Li and O_2 that yields Li_2O_2 (lithium peroxide) as the discharge products.

With the appropriate electrolyte (e.g., ether-based electrolytes) [7–13], the formation of Li_2O_2 as the main reaction product of Li-air cell is highly probable during the oxygen reduction reaction (ORR). Depending upon the applied current density, the variation in the electron transfer rate determines the growth process of Li_2O_2 on the cathode [13]. In addition, the Li_2O_2 discharge product morphology and crystallization can be a function of several parameters that are dictated by the electrolyte, Li- and O_2 -mass transport, O_2 partial pressure, rate of nucleation/precipitation and dissolution, catalyst, and chemical potential gradient interaction with the various carbon surfaces at the atomistic level due to the complex three-phase-boundary (*i.e.*, electrolyte-gas-solid electrode) condition (Figure 1A) in Li-air cells. To investigate the growth and morphology of Li_2O_2 discharge products in Li-air cells, the results of precisely controlled size-selective nanometer transition metal clusters decorated Li- O_2 cell cathodes has been reported recently [12]. By considering the possible thermal fluctuations and external driving forces due to an applied voltage on the cathode during the operation of a Li-air cell, it is thus reasonable to assume that the electrochemical growth and crystallization of Li_2O_2 may deviate from its thermodynamic equilibrium ground state, and resemble various possible competing crystalline or amorphous structures, or resemble a mixture of Li_2O_2 solid phases with various configurations that deviate from the thermal equilibrium ground state. Therefore, a systematic computational study of possible metastable Li_2O_2 crystalline phases can help provide insight into the various possible structures of Li_2O_2 to help the development of Li-air battery batteries.

In spite of its great importance for Li-air batteries, the possible lattice structures of lithium peroxide has not been extensively studied. As is well known, the reactivity of Li-metal with respect to oxygen is very high and in principle, can form various Li-O compounds, depending on the oxidation states and complexes of dioxygen (assuming cleavage of O-O bond is not energetically favorable) coordinating to Li ions. For Li_2O_2 , in which the metal-dioxygen complexes are usually classified as peroxo complexes [14],

the crystallographic structure has been proposed based on experimental XRD studies during the 1950s [15,16]. Based on Feh *et al.* [16] and Föppl [15] interpretations from the XRD studies, two different descriptions of the lithium peroxide crystalline structures can be proposed. To account for the fact that lithium is a poor X-ray scatterer and that the crystallinity of lithium peroxide might not be determined by XRD, its crystalline structure has recently been determined by Cota *et al.* [17] based on density functional theory (DFT). According to Cota *et al.* [17], the two proposed Li_2O_2 crystal structures based on the XRD interpretation [15,16], which are both ascribed to a $P\bar{6}$ space group, can both be described by a $P6_3/mmc$ space group. The DFT results favored the lithium peroxide crystal structure proposed by Föppl [15] over the structure proposed by Feh *et al.* [16]. Since then, subsequent theoretical studies of the Li_2O_2 crystalline structure have only focused on the Föppl structure [18–27]. The most recent effort in determining the commercially available Li_2O_2 powder crystalline structure among the Föppl and Feh *et al.* structures was reported by Chan *et al.* [24]. There are no systematic studies of the possibility of the existence of other metastable structures of Li_2O_2 .

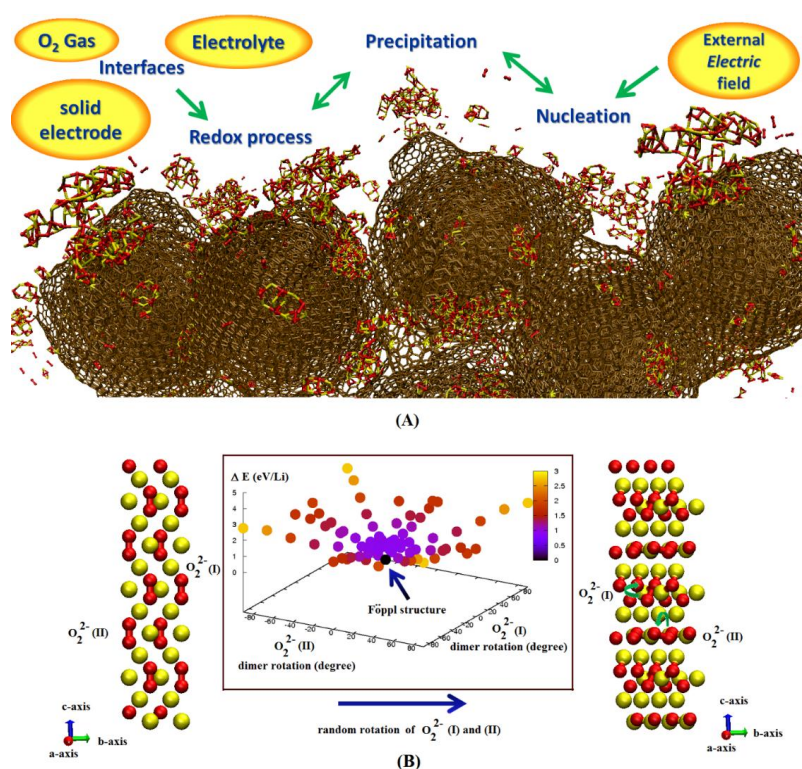


Figure 1. (A) A schematic description of the complex environment that might be involved in Li_2O_2 growth in a Li-air cell; (B) A three-dimensional plot of total energy fluctuation (*i.e.*, ΔE in eV/Li) for various possible configurations that deviate from the lowest energy structure, *i.e.*, Föppl structure due to the degrees of freedom involving O_2^{2-} ion rotations within the crystal lattice. The oxygen, lithium and carbon atoms are shown in red, yellow and brown color, respectively.

In this work, we seek to study several low energy structures of Li_2O_2 crystals using first-principles and ab initio thermodynamic approaches to explore their relative thermodynamic stabilities, structural properties, lattices dynamics, dielectric properties, and electronic properties. In order to compare with the results of current experimental characterization techniques, the simulated X-ray diffraction (XRD)

of several low energy crystalline phases of Li_2O_2 are presented, together with their neutron scattering structure factors, atomic vibration phonon dispersion spectra, and electronic properties.

2. Results and Discussion

2.1. Generation of Structural Models of Metastable Li_2O_2 Structures

To date, a detailed atomistic characterization of the Li_2O_2 system grown on the electrode of Li-O₂ cell has not yet been reported. Therefore it is reasonable to assume that lithium peroxide might exhibit several metastable structures, in addition to the commonly known ground state Föppl structure, which can be found in commercial Li_2O_2 powders. In a Li_2O_2 crystal within the well-known Föppl structure, the peroxide ions (*i.e.*, O_2^{2-}) can be identified by its characteristic Raman signature at $\sim 795\text{ cm}^{-1}$ that corresponds to stretching mode of the peroxy O-O bond [23]. The strong localized electron-hole (e-h) pairs that lead to strong vibronic coupling in the optical properties of Li_2O_2 [26] suggest that it could be treated as a molecular solid. For a Li_2O_2 solid grown in an operating Li-O₂ cell, the fundamental O_2^{2-} peroxy ions, in principle, can possess various random rotational orientations during the electrochemical synthesis and thermodynamic processes, coupled in parallel with the random influx of Li^+ ions in the system, as shown in Figure 1A.

Given this consideration, the orientation of the O_2^{2-} peroxy ions can be comprehended as one of the key components in determining the basic structural motif of Li_2O_2 crystalline lattice when coupled with Li^+ ions. Thus, the orientation of O_2^{2-} peroxy units can be used as a simple atomic displacement parameter to explore the local potential energy surfaces around the ground state Föppl structure and subsequently generate several metastable structures. As shown in Figure 1B, the well-ordered -Li-O-Li-O- atomic planes in a crystal cell can be altered by random orientation of O_2^{2-} ions in a crystal unit cell to obtain several new metastable structures of Li_2O_2 based on DFT simulations. For a ground state Li_2O_2 crystal in $P\bar{6}$ space group according to the Föppl structure, both O_2^{2-} dimers (*i.e.*, O_2^{2-} (I) and O_2^{2-} (II)) embedded in the lattice of Li^+ ions are found to align their molecular axis along the *c*-direction, as shown in Figure 1B. By fixing the crystal lattices initially, an approximate potential energy surface scan with random O_2^{2-} ions orientation can be obtained as shown in Figure 1B. By defining the $\Delta E = E_{\text{O}_2^{2-}(\text{random})}^{\text{tot}} - E_{\text{O}_2^{2-}(\theta=\text{along } c\text{-axis})}^{\text{tot}}$, as anticipated in Figure 1B, the approximate landscape of the total energy fluctuation (ΔE) can span $\sim 3.0\text{ eV/Li}$ above the ground state Föppl structure. Within the vicinity of $\Delta E \sim +0.50\text{ eV/Li}$, we found the preferred random orientation of the O_2^{2-} ions at $\theta \sim \pm 20^\circ$ along the *c*-axis of crystal lattice. With $\theta \leq 35^\circ$ for the random orientation of the individual O_2^{2-} peroxy ions as the initial configuration, the relaxed configurations of Li_2O_2 crystal are generally found to be Föppl-like structures with some distortions (e.g., structure-IV in Figure 2). For other structures, the optimized structure can be obtained after further cell lattice relaxation together with internal atomic coordinate optimizations.

2.2. Relative Thermodynamic Stability of the Metastable Li_2O_2 Crystal Structures

As shown in Figure 2, the O_2^{2-} ions orientation with respected to *c*-direction varies among different crystal structures. However it is noteworthy to point out that the orientation of O_2^{2-} ions with its molecular bond axes that deviated from the *c*-direction is not unusual among the alkali metal peroxides. For example, K_2O_2 favors the O_2^{2-} molecular axis deviating with an angle of $\theta \sim 45^\circ$ from the *c*-axes in the orthorhombic

lattice. However we found that for the lighter alkali metal (*i.e.*, Li) embedded in a crystalline lattice, the O_2^{2-} ions in general have less energetic preference to rotate away from the *c*-axes (*i.e.*, $\theta \neq 0$) in the crystal lattice compared to what we found in the K_2O_2 *Cmce* crystal lattice [28]. From our DFT results, the Gibbs free energy of the Li_2O_2 crystal in the *Cmce* lattice (*i.e.*, structure-III) is ~ 2.81 eV/Li at ambient conditions (*i.e.*, $T = 298$ K at 1.0 atm. P_{O_2}), which is slightly less stable than the Föpl structure (*i.e.*, ~ 2.86 eV/Li). In contrast to the Föpl structure, which favors all the O_2^{2-} dimers in the same orientation along *c*-axes of the crystal lattice (Figure 1B), in the orthorhombic *Cmca* phase as one moves along the *c*-axes in the crystalline lattice all the O_2^{2-} ions in one layer are rotated in the clockwise direction; in the next layer, the peroxide ions are rotated in the anticlockwise direction.

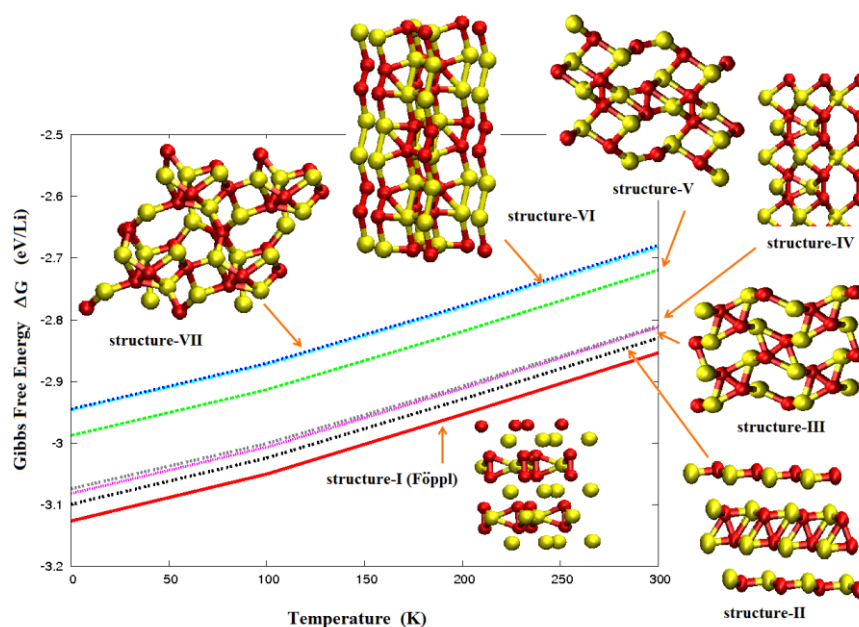


Figure 2. Selected Li_2O_2 crystal structures found in simulations that are metastable with respect to the Föpl structure (*i.e.*, structure-I) in terms of Gibbs free energy, ΔG (eV/Li) in the low temperature regime (*i.e.*, $T \leq 300$ K).

Through exploration of the potential energy surface derived from the random orientation of O_2^{2-} ions (Figure 1B), several other new low energy Li_2O_2 crystal structures were found in the vicinity of $\Delta G \sim 0.20$ eV/Li, as shown in Figure 2 and Table 1. Among the newly found low energy structure is structure-II (Figure 2), which is only ~ 0.03 eV/Li less stable than the Föpl structure, with the initial O_2^{2-} molecular axis deviating by an angle of $\theta \sim 75^\circ$ from the *c*-axes. After the geometry optimization, the relaxed structure favors low symmetry in a triclinic lattice. Here it is worthwhile to point out that the original structure proposed by Fehér *et al.* [16] in the $P\bar{6}$ representation is not stable compared to Föpl structure after geometry relaxation. The symmetry constrained structural relaxation of Fehér structure reported in previous studies [17,24] is confirmed to be $\Delta E \sim 0.29$ eV/Li (or ~ 0.58 eV/unit) energetically less favorable than the Föpl structure, and this symmetry constrained optimized structure is confirmed to be dynamically unstable due to a few imaginary phonon frequencies at the Brillouin Zone center (Γ -point). However by lifting the symmetry constraint and slightly changing the O_2^{2-} ions' orientation from the *c*-axes in crystal lattice, a stable crystalline phase of Li_2O_2 (*i.e.*, the modified Fehér structure or structure-VI in triclinic phase in Figure 2) can be obtained with $\Delta G \sim +0.18$ eV/Li at $T = 298$ K relative to the Föpl

structure. Considering that the discharge voltage in most Li-O₂ cells are typically several tenths of an eV below the thermodynamic equilibrium for the formation of ground state Föppl structure (*i.e.*, structure-I), the formation of these metastable Li₂O₂ crystal structures appear to be thermodynamically feasible.

Table 1. The crystal lattice constants, atomic density and Gibbs free energy of the selected thermodynamic stable crystalline structures of Li₂O₂ solids shown in Figure 2.

System (Li ₂ O ₂ crystalline structure)	Lattice constants (<i>a</i> , <i>b</i> , <i>c</i> in Å)	Atomic density (Crystal cell) (g/cm ³)	Gibbs free energy, Δ <i>G</i> (eV/Li) (<i>T</i> = 298 K and 1 atm <i>P</i> _{O₂})
I	3.13 (<i>a</i> = <i>b</i>), 7.62	2.37	−2.86
II	4.22, 3.47, 5.62	2.16	−2.83
III	3.46, 3.94, 5.23	2.14	−2.82
IV	3.11(<i>a</i> = <i>b</i>), 7.90	2.32	−2.81
V	3.15, 4.12, 5.68	2.21	−2.72
VI	3.29 (<i>a</i> = <i>b</i>), 7.34	2.17	−2.69
VII	6.01, 5.61, 3.93	2.08	−2.68

As shown in the Table 1, the crystal cell of the computed Li₂O₂ crystals varies and the differences in the atomic density can vary as much as ~14%. For the thermodynamically most stable Föppl structure (*i.e.*, Δ*G* ~ −2.86 eV/Li at *T* = 298 K at Figure 2), the atomic density of the primitive cell is ρ_{cell} ~ 2.37 g/cm³ and is the most dense among the various structures considered in this work.

The second lowest energy structure (*i.e.*, structure-II) has ρ_{cell} ~ 2.16 g/cm³ or ~9.7% less compact than the Föppl structure. For structure-III in an orthorhombic lattice, which resembles a K₂O₂-like phase in *Cmce* symmetry, the primitive cell density is also loosely packed with ρ_{cell} ~ 2.14 g/cm³. Relative to the Föppl structure, the modified Fehér structure (*i.e.*, structure-VI) is relatively sparse with ρ_{cell} ~ 2.15 g/cm³. For these Li₂O₂ systems, the basic structural properties can be studied by examining atomic correlations described by pair distribution functions, *g*(*r*), and angular distributions (Figure 3). The total neutron weighted pair distribution functions *S_M*(*q*) of these system are shown in Figure 4.

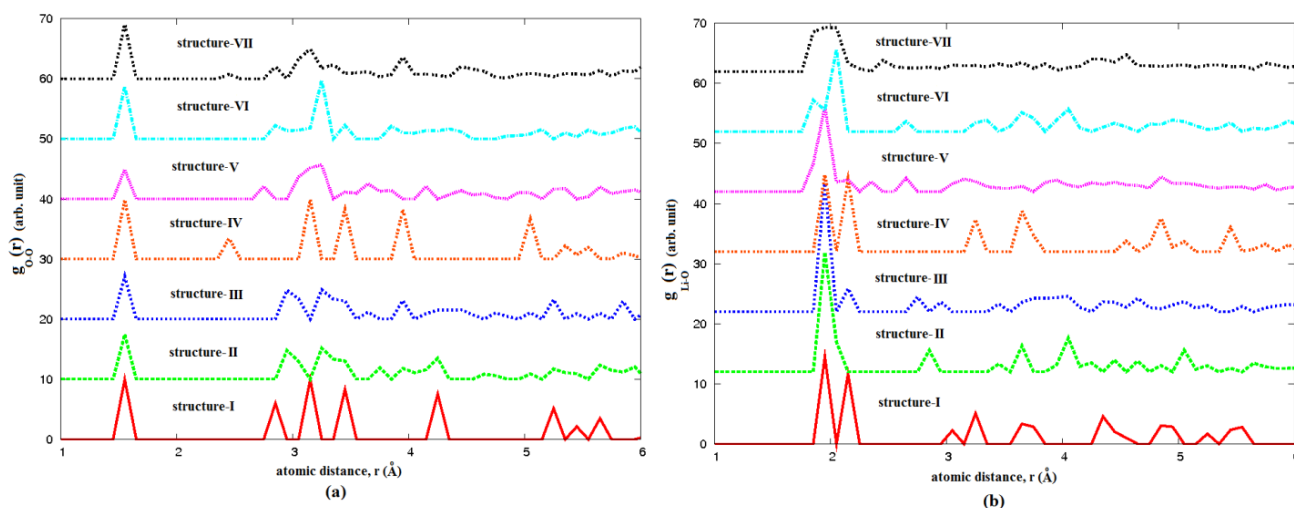


Figure 3. Cont.

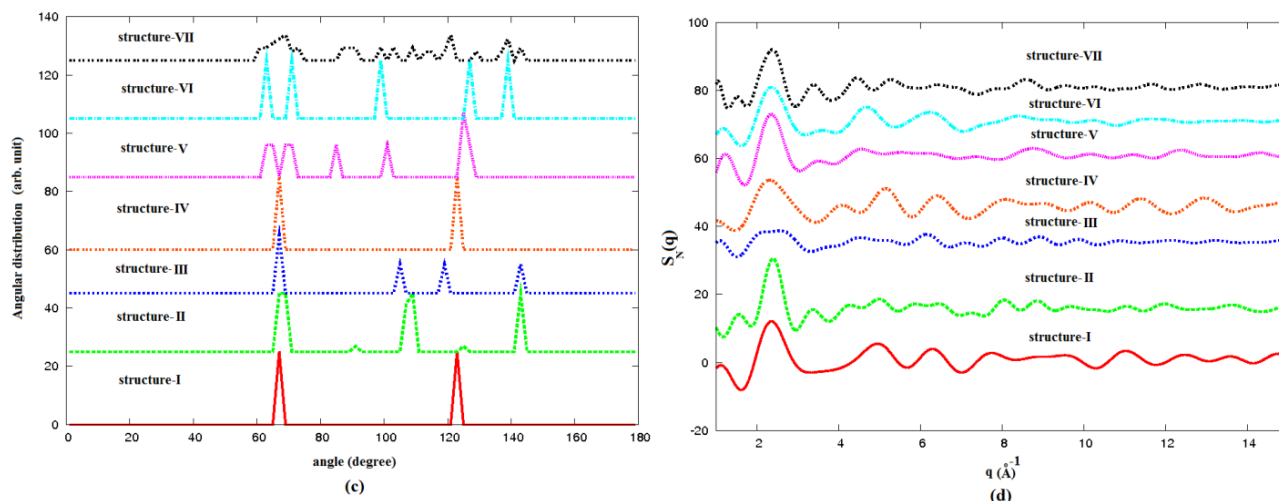


Figure 3. The Li_2O_2 crystal structures pair distribution function $g(r)$ of (a) O-O (*i.e.*, $g_{\text{O-O}}(r)$); (b) Li-O (*i.e.*, $g_{\text{Li-O}}(r)$); and the corresponding angular distribution function of (c) Li-O-O bonds; and (d) calculated neutron static structure functions for these Li_2O_2 system.

From $g(r)$ in Figure 3, the position of the first peak in these curves is the Li-O and O-O nearest neighbor distances within the first coordination shell. In contrast to Li-O coordination, the O-O bonds in these Li_2O_2 crystals are very similar regardless of distinctive crystal symmetry and lattices. Compared to the Li-O coordination shell, the very narrow distribution of O-O first coordination shell among these Li_2O_2 solids is attributed to the unique O-O covalent bond of O_2^{2-} ions in these systems. As shown in Figure 3, this narrow distribution of O-O pair correlation gives the peroxide ions bond length to be $\sim 1.50\text{--}1.56 \text{ \AA}$, similar to that of the rigid O_2^{2-} dimer embedded in Li_2O_2 solid. In contrast, the broad distribution of Li-O (*i.e.*, Li-O distances $\sim 1.82\text{--}2.55 \text{ \AA}$) pair correlations is attributed to the various orientations of the O_2^{2-} ions coupled to Li^+ ions within the crystal lattices, and can be correlated to broad distribution of bond angle of Li-O-O depicted in Figure 3. To better correlate with experiment, these basic interatomic bonds can be projected in reciprocal space in terms of diffraction patterns (e.g., the neutron static scattering factor, $S_N(q)$) calculated as the Fourier transform of $g(r)$, which shown in Figure 3d. From Figure 3d, the low q -parts are related to intermediate-range order, whereas the first peak at peak $q \sim 2.5 \text{ \AA}^{-1}$ corresponds to nearest neighbor Li-O, O-O and Li-Li correlations. As anticipated in Figure 3d, the structure factor of the Li_2O_2 crystalline phases in general look similar suggesting the average atomic coordination shells of these solids are close to each other, but not identical. Above all, the $S_N(q)$ of the Föppl structure (structure-I) and the structure-IV (*i.e.*, the distorted Föppl structure) are alike as shown in Figure 2, reminiscent of the similarity for $g(r)$ of Li-O and O-O.

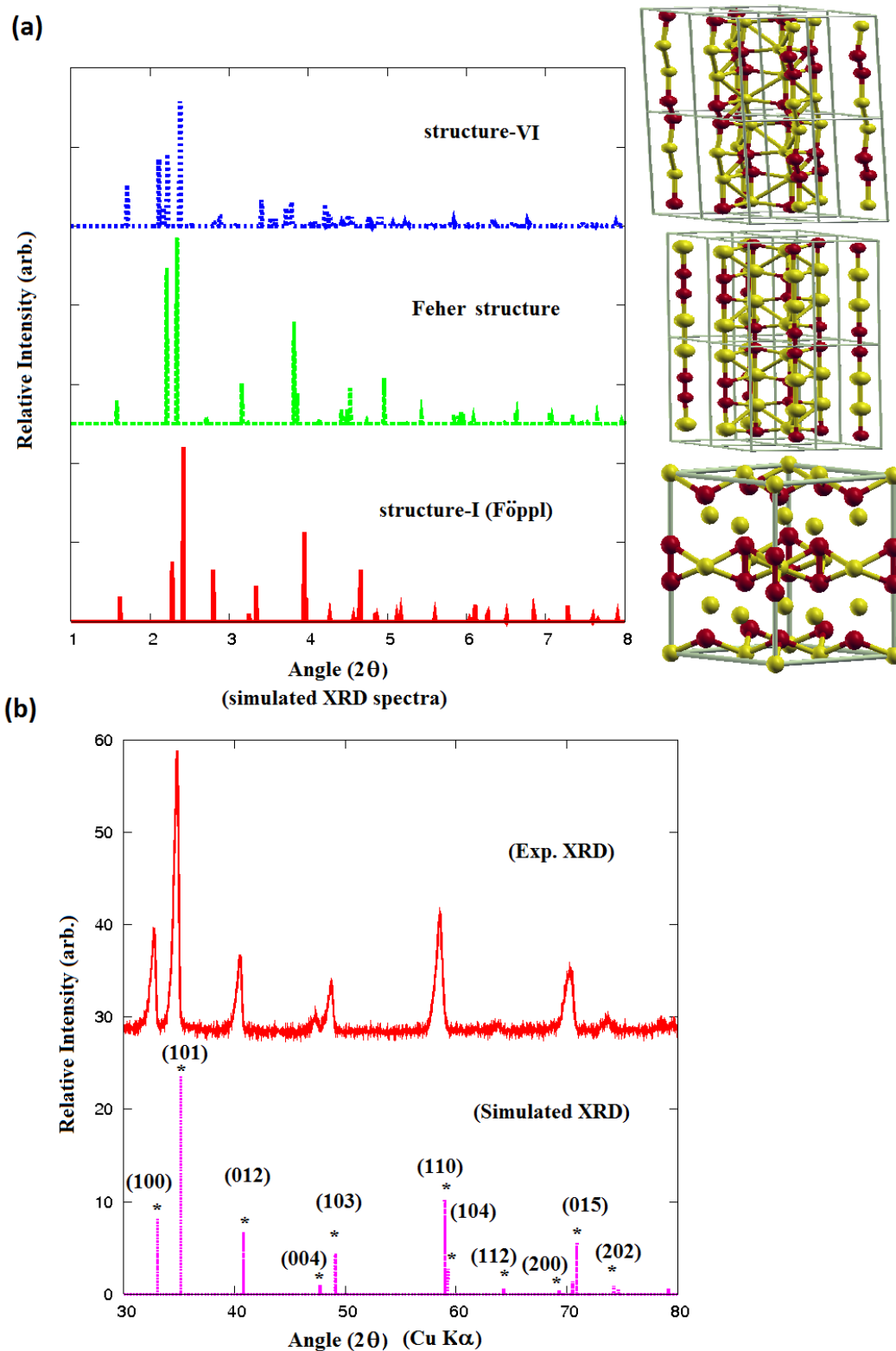


Figure 4. (a) The simulated XRD of the Föpl structure), the originally proposed Feher structure [17], and structure-VI (*i.e.*, the modified Feher structure) based on the X-rays wave-length, $\lambda = 0.10798 \text{ \AA}$, the same as in a previous experimental study [24]; (b) The experimental XRD of a commercial Li_2O_2 (Sigma-Aldrich) powder compared with the simulated XRD of the Föpl structure (X-rays wave-length, $\lambda = 1.5406 \text{ nm}$).

2.3. XRD Properties

To continue probe the fundamental structural properties of these Li_2O_2 crystalline phases, we next focus on the structural analysis based on X-ray diffraction (XRD) patterns. Through XRD, the quantification of crystal cell units, lattice constants, and phase identification of Li_2O_2 solids is feasible, assuming a bulk crystalline features are present. However it is important to point out that the determination of the Li_2O_2 structure through XRD alone sometimes can be ambiguous and insufficient (if there is no other complementary experimental characterization to support it), as in the following two examples.

According to Fister *et al.* [24], the experimental XRD patterns of the both Föpl and Fehér structure are nearly the same, and the minor difference can only be distinguishable through the measured residuals (*i.e.*, the differences between the Rietveld refinement and observed intensities). In order to confirm this finding, the simulated XRD patterns of the Föpl structure (*i.e.*, structure-I in Figure 2) and the originally proposed Fehér structure (*i.e.*, in $P\bar{6}$ representation) are computed based on a high energy 114.82 keV X-ray wave-length ($\lambda = 0.10798 \text{ \AA}$) [24] as shown in Figure 4. As anticipated in Figure 4, the simulated XRD patterns of these two structures are nearly the same, consistent with the Fister *et al.* experimental findings [24].

In addition, ambiguity in experimental XRD references in a Li_2O_2 -like discharge product obtained from Li-air experimental samples can be a problem in interpretation. In a commercial Li_2O_2 powder, the lowest energy Föpl structure is obtained by chemical reaction of a mixture of lithium hydroxide (e.g., $\text{LiOH} \cdot \text{H}_2\text{O}$) and aqueous hydrogen peroxide (H_2O_2) after high temperature filtration [29]. In this case, the formation of the Föpl Li_2O_2 structure is most probably governed by the homogeneous nucleation from an aqueous solution. As shown in Figure 4, the high crystallinity of the Li_2O_2 in the Föpl structure is confirmed with a perfect matching among the simulated and experimental XRD patterns and their relative intensities. In contrast, for a crystalline entity of Li_2O_2 obtained from a discharge product in Li-air cell, the formation of a Li_2O_2 product probably involves heterogeneous nucleation from nonaqueous electrolytes in a polarized thermodynamic nonequilibrium media and at an electrified interface. Besides the huge differences in reaction kinetics, the thermodynamic Gibbs free energy that dictates the crystallization and nucleation process can be substantially different in both cases. Therefore in a Li-air cell environment, the electrocrystallization of Li_2O_2 solids can possibly consist of several forms of metastable Li_2O_2 structures, instead of the thermodynamically driven Föpl structure. In order to test this hypothesis, the supposition of the simulated XRD patterns of a few selected thermodynamic stable phases of Li_2O_2 with a Boltzmann weight from Figure 2 is plotted against the experimental XRD of a Li_2O_2 -like discharge product in Figure 5.

As shown in Figure 5, the experimental XRD of the discharge product obtained from the Li-air cell is Li_2O_2 -like, but not exactly as the same as the experimental XRD of the commercial Li_2O_2 powder (Figure 4). In contrast to the observed high crystallinity of commercial Li_2O_2 powder XRD, the XRD patterns of the discharge product are generally broader and lower in symmetry. As shown in the enlarged region of the XRD pattern (Figure 5) within the scattering angle of $32^\circ \leq 2\theta \leq 42^\circ$, there are a lot of XRD peaks within a range that cannot be simply correlated to the two iconic XRD peaks (*i.e.*, (100), (101)) mainly derived from the Li_2O_2 in Föpl structure. Rather they are from other metastable crystalline or amorphous Li_2O_2 structures. As shown, the presence of some unknown metastable Li_2O_2 structures cannot be ruled out based on the standard XRD patterns. This suggests that in order to interpret the basic

structural properties of a Li_2O_2 compound obtained from electrochemical discharge product of Li-air cell, referring to a single XRD reference based on the Föppl structure alone might not be sufficient.

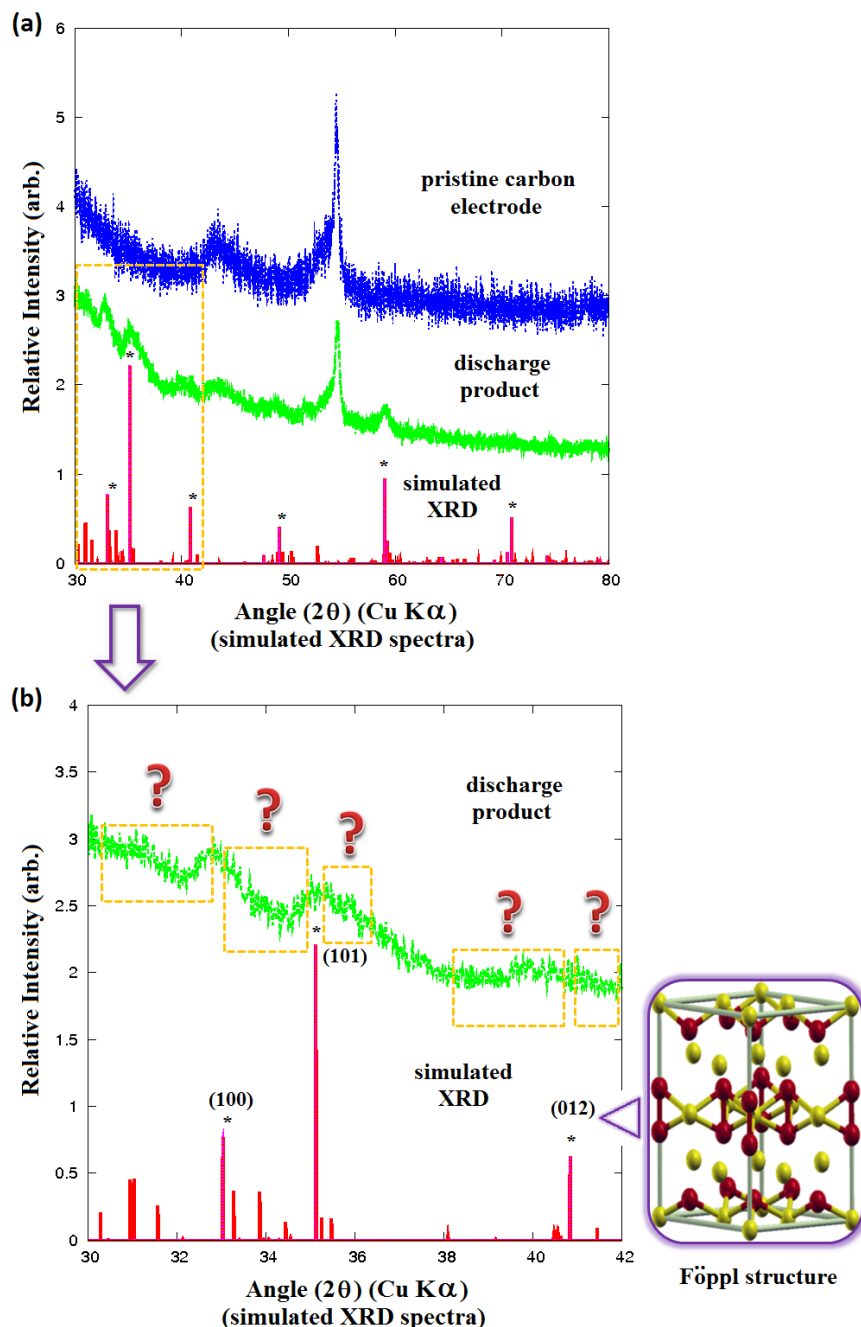


Figure 5. (a) The experimental XRD of a pristine carbon electrode and discharge product referenced to a simulated XRD Boltzmann weighted for a few metastable Li_2O_2 structures from Figure 2 together with Föppl-structure marked with an *-symbol; (b) The enlarged region (*i.e.*, $32^\circ \leq 2\theta \leq 42^\circ$) of the XRD data suggests the presence of Li_2O_2 metastable structures.

2.4. Atomic Vibrations and Phonons

The *ab initio* atomic vibration spectra of various Li_2O_2 solids represented by phonon dispersion and phonon density of states were calculated and are presented in Figure 6.

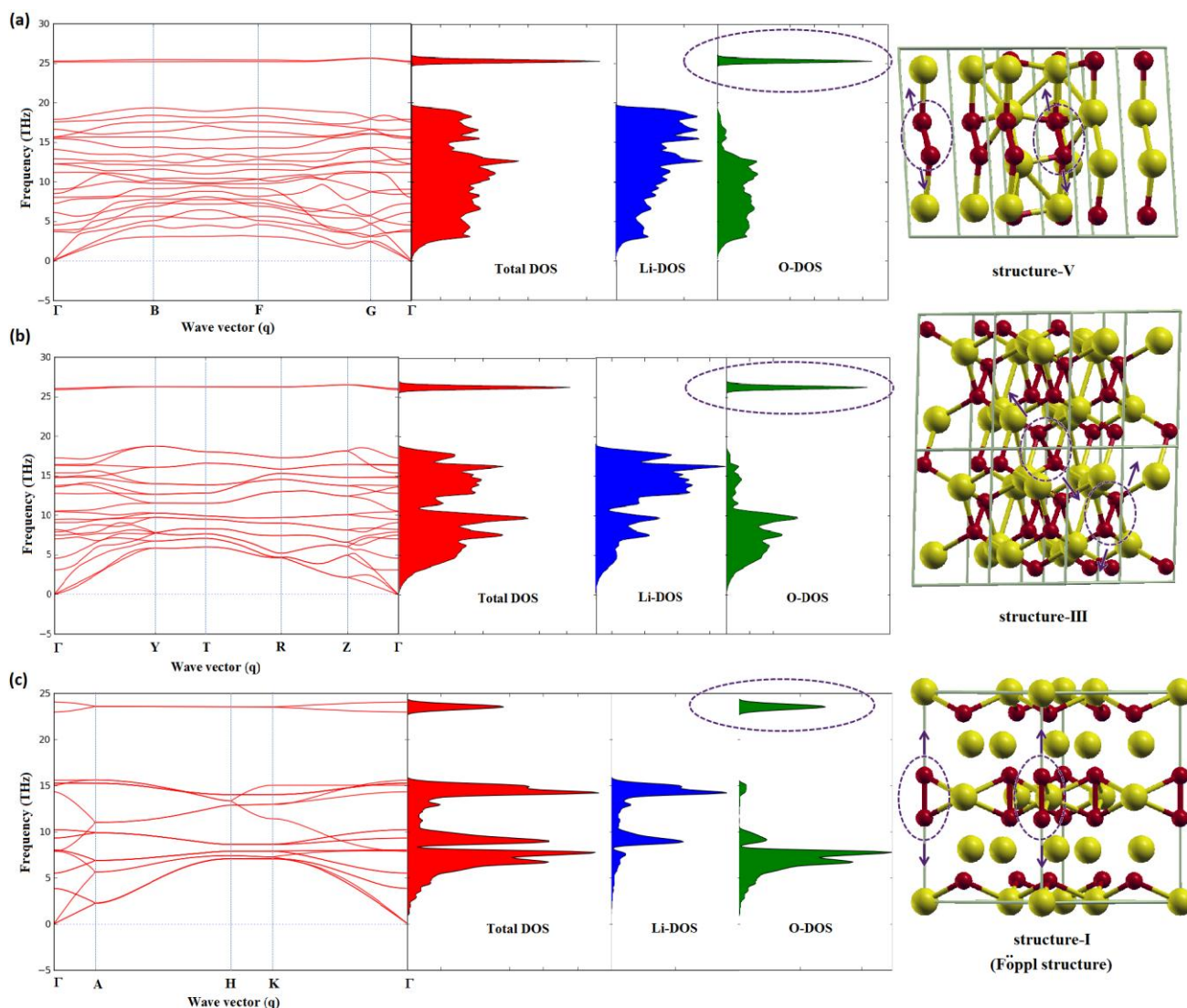


Figure 6. The phonon dispersion and phonon density of states (DOS) (*i.e.*, total DOS in red, Li-DOS in blue, and O-DOS in green color) of three representative Li_2O_2 crystalline phases: (a) structure-V in $P1$ space group; (b) structure-III in $Cmce$ space group and (c) structure-I (Föppl structure in $P\bar{6}$ space group). The purple highlighted DOS is the common signature of O-O stretching of an O_2^{2-} anion in the lattice.

This provides theoretical predictions for future experimental studies, especially for inelastic neutron scattering of unknown Li_2O_2 crystalline structures. To assist in the comparison, only selected phonon dispersion curves $\omega(q)$ in the wavevectors space across the first Brillouin zone of some Li_2O_2 structures are shown. For the thermodynamically most stable Li_2O_2 phase in the Föppl structure, the phonon branches are examined along Γ -, A-, H-, and K-points following the $P\bar{6}$ space group. The same equivalent structure in $P6_3/mmc$ space group yields similar phonon properties as expected [23]. No imaginary phonon modes can be found at the zone center and at other direction in the BZ suggesting that this peroxide crystal phase is dynamically stable. Compared to the other Li_2O_2 crystal structures that are lower in symmetry (e.g., structure-III and structure-V in Figure 6), the phonon dispersion of the Föppl structure is comparatively less scattered across BZ and yields a relatively localized phonon density of states (DOS). In general, the more scattered the Li-O bonds distribution (Figure 3) in a low symmetric

Li_2O_2 crystalline phase, the more the degeneracy of lattice vibrations are lifted resulting in more diffuse phonon dispersion and delocalized phonon DOS in the distribution (e.g., structure-III and -V).

Despite having different peroxide (O_2^{2-}) ions alignments, orientations and symmetries in crystal lattices, some common character in the atomic lattice vibration of these peroxide crystals can be found from the simulations. It is important to note that for a Li_2O_2 crystalline solid with an arbitrary symmetry (Figure 2), all the phonon modes are generally below ~ 27 THz (or ~ 900 cm^{-1}). From all the lattice dynamically stable Li_2O_2 crystalline structures we found, the oxygen anion (O_2^{2-}) vibration contribution can only be found at low and high frequency regimes that are separated by a gap in phonon DOS (Figure 6). The Li-O phonon coupling can be found at frequency regimes below ~ 20 THz (or ~ 660 cm^{-1}). For all the Li_2O_2 crystalline solids, the unique decoupling of the peroxide ions from the rest of lattice can be represented by a gap of ~ 20 – 25 THz in the phonon DOS (Figure 6). The highest frequency phonon modes are exclusively dominated by O-O stretching modes (~ 24.2 – 26.0 THz or ~ 799 – 865 cm^{-1}), characterized by a sharp oxygen phonon DOS peak (Figure 6) at the high frequency regime analogous to their common first nearest neighbor O-O bond as found in $g_{\text{O-O}}(r)$ shown in Figure 3 and the experimentally observed Raman intensity (*i.e.*, $\omega \sim 790$ cm^{-1}) [30–32]. In addition, these unique O-O stretching modes are close to the reported Raman spectrum of all the alkali and alkali-earth peroxides (~ 790 – 863 cm^{-1}) [33,34], which appear to be a common signature of a peroxy species (Figure 6) embedded in a molecular crystal lattice surrounded by Li^+ ions.

2.5. Dielectric Properties

From the computed atomic vibrations in the lattices mentioned above, the collective displacements of the constituent atomic motion contribute to the low frequency dielectric response of the Li_2O_2 bulk as an intrinsic macroscopic property. It is important to note that for Li_2O_2 formed during the discharge process of an Li-air cell cathode, its relative permittivity or the dielectric constant may directly control the charge capacitive properties, effective charge screening at the electrode/electrolyte interfaces, and the subsequent effective ionic current of this electrochemical device. So far, there is no reported experimental value of dielectric constant of Li_2O_2 in the literature, and the computed high frequency (ϵ^∞) and static dielectric constants (ϵ^0) of Li_2O_2 are presented in Figure 7. To simplify the discussion, only the orientationally averaged high frequency dielectric constants from the electronic contribution ($\langle \epsilon^\infty \rangle$) and static dielectric constants from the lattice contribution ($\langle \epsilon^0 \rangle$) of some structures will be discussed. We also report calculated dielectric constant data of Li_2O crystal in Figure 7 for comparison with Li_2O_2 .

Due to small differences in the atomic vibrational frequencies and the ionic distributions in phonon density of t (Figure 6), only a small variation of the computed $\langle \epsilon^\infty \rangle$ and $\langle \epsilon^0 \rangle$ among the various Li_2O_2 structures can be found (Figure 7) despite the substantial difference in crystal symmetry. From our results, Li_2O_2 is predicted to be a high- k material relative to SiO_2 ($\epsilon \sim 3.5$) [35]. The sum of orientationally averaged $\langle \epsilon^\infty \rangle$ and $\langle \epsilon^0 \rangle$ of Li_2O_2 crystal with various phases is found to be within a range of $\epsilon \sim 7.2$ to 9.4 . For the Li_2O crystal the sum of orientationally average $\langle \epsilon^\infty \rangle$ and $\langle \epsilon^0 \rangle$ is $\epsilon \sim 7.5$, close to the experimentally reported $\epsilon \sim 6$ based on microwave dielectric constant measurement [36]. The high frequency dielectric constant $\langle \epsilon^\infty \rangle$ of Li_2O_2 appears to be ~ 2.6 to 3.2 , relative to 2.9 of Li_2O . For the static dielectric constant $\langle \epsilon^0 \rangle$ of Li_2O_2 attributed to the lattice contribution, the values are within the range of ~ 4.6 to 6.2 relative to 4.6 of Li_2O .

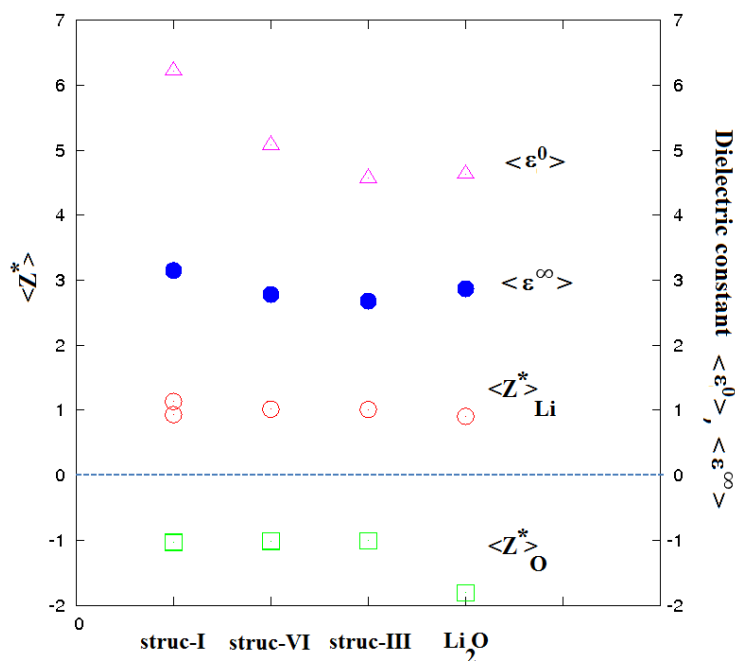


Figure 7. The computed orientationally averaged static dielectric constants of lattice contribution $\langle \epsilon^0 \rangle$ and electronic contribution $\langle \epsilon^\infty \rangle$; and isotropically averaged of atomic Born charges, $\langle Z^* \rangle$ of Li and O for few selected structures of Li_2O_2 : structure-I (struc-I), III (struc-III), VI (struc-VI). Calculated results for the Li_2O crystal are also included for comparison.

The similarity of the dielectric responses of Li_2O_2 and Li_2O can be understood based on the computed atomic Born effective charges (Z^*) [37,38] of the constituent Li- and O-atoms in both systems, which determines the dielectric tensor, $\epsilon_{\alpha\beta}^0 = \epsilon_{\alpha\beta}^\infty + \frac{4\pi e^2}{V} \sum_i \frac{Z_{i\alpha}^* Z_{i\beta}^*}{\omega_i^2}$ with V being the crystal unit cell volume, and ω_i being the phonon frequencies of IR-active modes [37]. The computed Z^*_i tensors of Li_2O_2 and Li_2O generally have no symmetry, and are dominated by the diagonal terms for most atoms. To present the Z^* data in a manageable way, Figure 7 is a scatter plot of just the isotropic averages (*i.e.*, one-third of the trace) of the atomic $\langle Z^* \rangle$ tensors sorted by atom type for the system. Overall, the sum of $\langle Z^*_i \rangle$ of all atoms in Li_2O_2 and Li_2O in each unit cell will vanish within numerical accuracy, obeying the charge neutrality sum rule [37]. From Figure 7, the $\langle Z^* \rangle_{\text{Li}}$ and $\langle Z^* \rangle_{\text{O}}$ of Li_2O_2 and Li_2O are very similar in magnitude relative to the nominal ionic valences of the isolated ions (+1, -2 and -1 for Li^+ , O in Li_2O and O in Li_2O_2). For Li_2O , the larger $\langle Z^* \rangle_{\text{O}}$ in a crystal cell does not increase the ϵ^0 as the oxide ion contribution in crystal cell is less relative to Li_2O_2 . No anomalously large Z^* values in these materials indicates that there is only a minimal dynamic charge transfer from the chemical bonds as the bond length varies during the perturbed displacements. The $\langle Z^* \rangle_{\text{O}} \sim -1.0$ in Li_2O_2 indicates that the unique peroxy species O_2^{2-} molecular dimer remains nearly rigid in the crystal lattice. Analogous to the similarity in the partial phonon density of states for the constituent atoms among the various Li_2O_2 phases, no significant differences of the $\langle Z^* \rangle_{\text{Li}}$ and $\langle Z^* \rangle_{\text{O}}$ can be found among the different structures of Li_2O_2 . The ϵ^0 of the structure-I (*i.e.*, Föppl structure) is slightly larger due to its smaller crystal unit cell and larger atomic density.

2.6. Electronic Properties

To determine whether Li_2O_2 solid is a molecular solid crystal, we analyzed the basic electronic structure properties of these systems in addition to the phonon and dielectric properties (Section II D and II E). For all of the thermodynamic and lattice dynamically stable Li_2O_2 crystals studied (Figures 2 and 6) in this work, we found all the Li_2O_2 crystalline solids to be nonmagnetic and insulating in its electronic properties, regardless of different peroxide ion (O_2^{2-}) orientation within the crystal lattice. This finding is consistent with a recent DFT study that predicted amorphous lithium peroxide to be amorphous with randomly oriented peroxy ions [39]. As expected, the band gap predicted by PBE is generally underestimated. For all of the Li_2O_2 solids studied we found (Figure 2), the PBE band gap to be ~ 1.8 – 2.1 eV. For the structure-I (Föppl structure), the more accurate HSE06 calculation predicts the band gap to be ~ 4.9 eV (Figure 8), close to the reported G_0W_0 band gap (*i.e.*, ~ 4.81 – 4.91 eV) [21,25,26]. The calculated electronic densities of states of two structures (I and III) are given in Figure 8. For the structure-III with different O_2^{2-} orientations, the predicted band gap is also found to be similar, *i.e.*, ~ 2.02 eV and ~ 5.08 eV respectively from PBE and HSE06 solutions. Thus this also suggests that without impurities, defects, vacancies, metallic mixed valence ($\text{O}_2^{2-}, \text{O}_2^-, \text{O}^{2-}$) disordered stoichiometric Li_2O_2 amorphous structures [11,22,25,40,41], polarons [21,27,39,42,43] or surfaces conduction [20,30,40,44] in these Li_2O_2 bulk crystal (Figure 2), electronic conduction is unlikely. As is evident from the DOS shown in Figure 8, the contribution from the Li-states below the Fermi level (E_f) is minor, indicating that Li behaves like an electron donor in these systems. In contrast, the contributions from O- p states dominate in the vicinity of E_f . As given in Figure 8, the total charge density contour plot shows that the electronic charge of the system is mainly populated around the O_2^{2-} dimer in the lattice. Through the Bader charge partition scheme [45], the ρ_{Li} and ρ_{O} of these systems are found to be $\sim +0.85$ e and ~ -0.85 e respectively, which provides support that the O_2 dimer is an O_2^{2-} -like anion and, therefore, equivalent to a peroxide ion within the Li^+ lattices.

To further support our hypothesis, we first examined the computed energy levels of the molecular orbitals and the corresponding DOS for a single peroxide ion (O_2^{2-}). Since the neutral O_2 triplet dimer contains two unpaired electrons in a π^* -antibonding orbital, in a peroxide ion, the spin moment vanishes ($S = 0$, singlet), with two extra electrons donated by neighboring Li^+ cations to the π^* -level. This explains why all the stoichiometric Li_2O_2 crystal solids are nonmagnetic insulators. Consequently, one also finds that the effective electrostatic repulsions among the two oxygen atoms within an O_2^{2-} dimer are stronger, and this yields a longer O-O bond distance for a peroxide ($R_{\text{O-O}} \sim 1.50$ – 1.56 Å) as suggested by the $g_{\text{O-O}}(r)$ from Figure 3 relative to a molecular O_2 dimer. The unique molecular character of an isolated O_2^{2-} is shown in Figure 8.

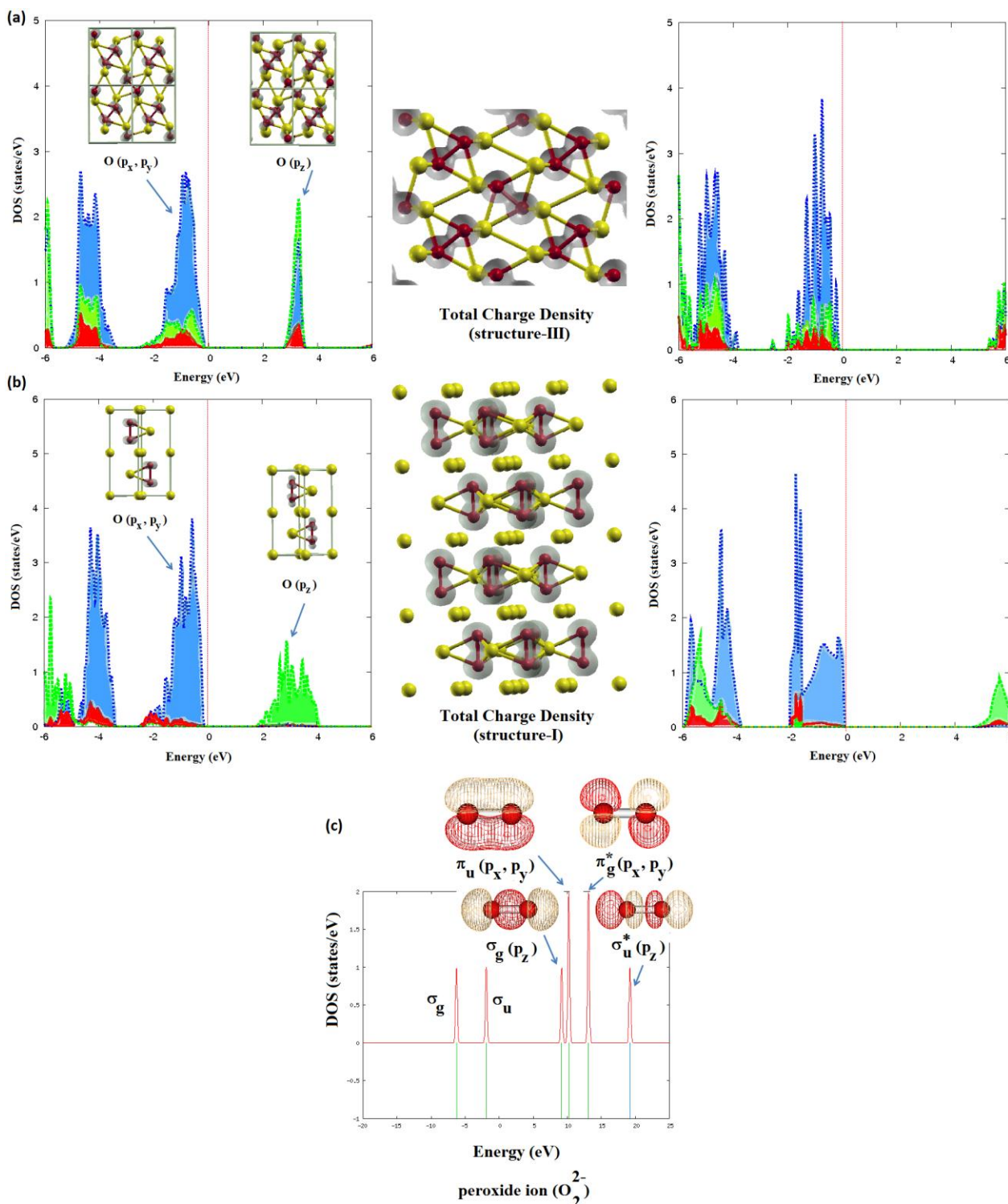


Figure 8. The electronic partial density of states (PDOS) of Li_2O_2 structure-III (a) and structure-I (b) for oxygen (p_x, p_y) (blue), p_z (green) and lithium (red) contributions from PBE (left) and HSE06 (right) calculations with the Fermi-level (E_f) set to zero. The inset is the figure of partial charge density (at an isovalue $\rho \sim 0.4 \text{ e}/\text{\AA}^3$) at the vicinity of E_f that mostly corresponds to oxygen p -character. The total charge density of the system (center) is set to be at an isovalue $\rho \sim 0.9 \text{ e}/\text{\AA}^3$; (c) The representative molecular orbitals and DOS of a peroxide ion O_2^{2-} in the PBE calculation. The green and blue-lines represent the occupied and unoccupied orbitals respectively in the system.

For an O_2^{2-} ion, the $\sigma_u^*(p_z)$ -level, *i.e.*, the lowest unoccupied molecular orbital (LUMO) and the $\pi_g^*(p_x, p_y)$ -level, *i.e.*, the highest occupied molecular orbital (HOMO) are separated by ~ 6.10 eV. The orbital-projected partial DOS to the top valence and lowest conduction bands of structure-I and structure-III of Li_2O_2 solids are shown (*i.e.*, the inset of Figure 8). The top valence bands of these two Li_2O_2 crystalline solids are very similar, *i.e.*, they have a π_g^* -like character that is exclusively governed by O- (p_x, p_y) in character. For the lowest conduction band, it is found to be σ_u^* -like dominated by O- (p_z) character for both structure-I and III Li_2O_2 crystals. Interestingly it reveals that for both crystalline structures, the distribution of the top occupied valence bands and the lowest unoccupied bands are also separated by ~ 5.0 – 6.0 eV, close to an isolated O_2^{2-} ion as found in the simulation. Thus, this suggests that the valence and conduction bands of these Li_2O_2 crystalline solids are almost exclusively determined by the unique electronic states of the individual peroxide ions embedded within the crystal lattice, and therefore are likely to be a molecular ionic solid. Thus, without the defects (e.g., dopants, atomic vacancy) in a Li_2O_2 crystal, the pristine O_2^{2-} electronic configuration seems to be stable and will not be destroyed by the hybridization with neighboring Li^+ in crystal lattice as long as the fundamental chemical stoichiometry of the basic crystallographic cell is conserved.

3. Methodology

3.1. Computational Method

In this work, all the DFT calculations were performed using the planewave DFT code VASP [46] with projector augmented wave (PAW) methods based on the generalized gradient approximation (GGA) Perdew-Burke-Ernzerhof (PBE) exchange-correlation functional. For comparison, some of the solutions are checked using the hybrid functional HSE06 for proper description of electronic band gap prediction. The planewave kinetic energy cutoff is 430 eV, and a mesh of $9 \times 9 \times 9$ was used for integration of the first BZ for Li_2O_2 bulk calculations. In all cases, the 2 s electrons for Li and the 2 s and 2 p electrons for O were treated as valence electrons, and the remaining electrons were kept frozen. The total energy convergence is set to be 1×10^{-6} eV and both cell parameters and internal atomic positions were optimized until the residual forces became less than 1×10^{-3} eV/Å. For the phonon calculations, the result is obtained using the phonopy code within the harmonic approximation [47]. For the investigation on thermodynamic stability at finite temperatures, the Gibbs free energy is computed as described in our previous work [23]. To predict the dielectric constant of Li_2O_2 , the second derivatives of the total energy of these periodic solids with respect to collective displacements of the constituent atoms with different wavevectors commensurate with the underlying lattice were computed with variational density functional perturbation theory as implemented in the VASP package [46].

3.2. Experimental Method

The Li_2O_2 discharge product was electrochemically formed in plastic Swagelok cells. The carbon cathode was based on activated carbon powders (80 wt %) and polyvinylidene fluoride binder (PVDF, 20 wt %) that were mixed in a solution of *N*-methyl-2-pyrrolidone (NMP) and coated on Toray carbon paper with a carbon loading density of ~ 1.6 mg/cm². The anode, electrolyte, and separator were lithium metal foil, 1.0 M $LiCF_3SO_3$ in TEGDME, and a glass fiber separator, respectively. The cell was sealed in

a glass chamber filled with 1 atm of high purity oxygen. All the electrochemical experiments are performed using a Maccor battery cycler at 298 K. For the galvanostatic charge test, the charging was terminated at an upper voltage of 4.5 V vs. Li or when the charge capacity was the same as the discharge value at current density of 0.1 mA/cm². The activated carbon (AC) powders used for the carbon electrode were prepared following the method described in our previous work [30]. For the XRD measurements, the discharged AC cathode was washed with TEGDME solvent in a glove box and dried at 90 °C under vacuum. The dried electrode was characterized by use of X-ray diffraction (XRD, Rigaku, Miniflex). In order to avoid exposure to air the discharged AC electrode was sealed on the glass holder using Kapton[®] film.

4. Conclusions

In conclusion, we have predicted various low energy structures of Li₂O₂ crystal solids that are both thermodynamically and lattice dynamically stable at ambient conditions with the commonly known Föpl structure of Li₂O₂ found still to be the most stable configuration. The O-O bond of O₂²⁻ peroxy ions in Li₂O₂ crystalline solid is shown to have the unique effects on its structural, electronic, vibrational and dielectric properties. In the exploration of the potential energy surface, we found that altering the orientation of O₂²⁻ peroxy ions can be a simple, yet powerful atomic displacement parameter in determining in the search for metastable Li₂O₂ crystalline structures. All the newly located Li₂O₂ crystal structures are found to be insulating and a high-*k* materials, with a common unique signature of an O₂²⁻ vibration mode ($\omega \sim 799\text{--}865\text{ cm}^{-1}$) as is observed in Li-air battery experiments, regardless of the random O₂²⁻ orientations and symmetry in the crystal lattice. From phonon and electronic properties analysis, the robustness of the O-O bond of O₂²⁻ peroxy ions seems to be a common signature of lithium peroxide crystal phase that suggest that Li₂O₂ is a molecular ionic solid in nature, and its fundamental properties seem to depend on the coupling and decoupling of the localized O₂²⁻ peroxy ions with the rest of Li⁺ ions from surrounding.

From calculated thermodynamic stabilities, the coexistence of different Li₂O₂ crystalline phases are feasible within a narrow range of chemical potential $\Delta G \sim 0.20\text{ eV/Li}$ or an equivalent discharge voltage window of $\sim 0.20\text{ V}$ from open circuit voltage in an Li-air electrochemical cell. In order to verify this prediction, we have proposed a combination of several experimental characterization techniques. The commercially available Li₂O₂ powder is confirmed to be the thermodynamic ground state Föpl-like structure. However, in order to determine the structures of the Li₂O₂ compounds electrochemically grown in a Li-air cell, we found that XRD patterns alone are not sufficient due to the poor crystallinity of the samples. In addition, the commonly known Raman signal of O₂²⁻ vibration mode is also found to be insufficient to determine these newly predicted Li₂O₂ crystal structures, as all of them have a similar O₂²⁻ vibration mode. Thus, more sophisticated characterization techniques that are sensitive to crystal symmetry and local atomic structures (e.g., EXAFS, non-resonant inelastic X-ray scattering (NIXS), neutron scattering spectroscopy, *etc.*) that can be coupled with in-situ time-resolved techniques are needed in the future experiments.

Acknowledgments

This work was supported as part of the Center for Electrochemical Energy Science, an Energy Frontier Research Center funded by the U.S. Department of Energy, Office of Science, Basic Energy Sciences under Award # DEAC02-06CH11357. The authors want to thank to Dengyun Zhai and Hsien-Hao Wang's

generosity by providing the electrochemically grown Li_2O_2 discharge product and commercial (Aldrich) Li_2O_2 powder for experimental XRD data. We also acknowledge grants of computer time through the allocations on the Center for Nanoscale Materials (CNM) Carbon Cluster at Argonne National Laboratory, the Argonne Leadership Computing Facility (ALCF) Fusion Cluster at Argonne National Laboratory, and the EMSL Chinook Cluster at Pacific Northwest National Laboratory.

Author Contributions

Kah Chun Lau was responsible for the theoretical computations. Jun Lu, Dantong Qiu, and Xiangyi Luo was responsible for the experimental part. Kah Chun Lau, Jeffrey Greeley, Larry A. Curtiss and Jun Lu wrote the manuscript. Larry A. Curtiss and Khalil Amine supervised the project. All of the authors discussed the results and reviewed the manuscript.

Conflicts of Interest

The authors declare no conflicts of interest.

References

1. Girishkumar, G.; McCloskey, B.; Luntz, A.C.; Swanson, S.; Wilcke, W. Lithium-air battery: Promise and challenges. *J. Phys. Chem. Lett.* **2010**, *1*, 2193–2203.
2. Christensen, J.; Albertus, P.; Sanchez-Carrera, R.S.; Lohmann, T.; Kozinsky, B.; Liedtke, R.; Ahmed, J.; Kojic, A. A Critical review of Li/Air batteries. *J. Electrochem. Soc.* **2012**, *159*, R1–R30.
3. Lu, J.; Li, L.; Park, J.B.; Sun, Y.K.; Wu, F.; Amine, K. Aprotic and aqueous Li- O_2 batteries. *Chem. Rev.* **2014**, *114*, 5611–5640.
4. Bruce, P.G.; Freunberger, S.A.; Hardwick, L.J.; Tarascon, J.M. Li- O_2 and Li-S batteries with high energy storage. *Nat. Mater.* **2012**, *11*, 19–29.
5. Choi, N.S.; Chen, Z.; Freunberger, S.A.; Ji, X.; Sun, Y.K.; Amine, K.; Yushin, G.; Nazar, L.F.; Cho, J.; Bruce, P.G. Challenges facing lithium batteries and electrical double-layer capacitors. *Angew. Chem. Int. Ed.* **2012**, *51*, 9994–10024.
6. Lu, J.; Amine, K. Recent research progress on non-aqueous lithium-air batteries from Argonne National Laboratory. *Energies* **2013**, *6*, 6016–6044.
7. Lau, K.; Assary, R.; Curtiss, L. Aprotic electrolytes in li-air batteries. In *Electrolytes for Lithium and Lithium-Ion Batteries*; Jow, T.R., Xu, K., Borodin, O., Ue, M., Eds.; Springer: New York, NY, USA, 2014; Volume 58, pp. 445–466.
8. McCloskey, B.D.; Scheffler, R.; Speidel, A.; Girishkumar, G.; Luntz, A.C. On the mechanism of nonaqueous Li- O_2 electrochemistry on C and its kinetic overpotentials: Some implications for Li-air batteries. *J. Phys. Chem. C* **2012**, *116*, 23897–23905.
9. Gallant, B.M.; Kwabi, D.G.; Mitchell, R.R.; Zhou, J.; Thompson, C.V.; Shao-Horn, Y. Influence of Li_2O_2 morphology on oxygen reduction and evolution kinetics in Li- O_2 batteries. *Energy Environ. Sci.* **2013**, *6*, 2518–2528.
10. Ottakam Thotiyl, M.M.; Freunberger, S.A.; Peng, Z.; Chen, Y.; Liu, Z.; Bruce, P.G. A stable cathode for the aprotic Li- O_2 battery. *Nat. Mater.* **2013**, *12*, 1050–1056.

11. Lu, J.; Lei, Y.; Lau, K.C.; Luo, X.; Du, P.; Wen, J.; Assary, R.S.; Das, U.; Miller, D.J.; Elam, J.W. A nanostructured cathode architecture for low charge overpotential in lithium-oxygen batteries. *Nat. Commun.* **2013**, *4*, 2383.
12. Lu, J.; Cheng, L.; Lau, K.C.; Tyo, E.; Luo, X.; Wen, J.; Miller, D.; Assary, R.; Wang, H.H.; Redfern, P.; *et al.* Effect of the size-selective silver clusters on lithium peroxide morphology in lithium-oxygen batteries. *Nat. Commun.* **2014**, *5*, 4895.
13. Adams, B.D.; Radtke, C.; Black, R.; Trudeau, M.L.; Zaghbi, K.; Nazar, L.F. Current density dependence of peroxide formation in the Li-O₂ battery and its effect on charge. *Energy Environ. Sci.* **2013**, *6*, 1772–1778.
14. Vaska, L. Dioxygen-metal complexes: Toward a unified view. *Acc. Chem. Res.* **1976**, *9*, 175–183.
15. Föpl, H. Die Kristallstrukturen der Alkaliperoxyde. *Z. Anorg. Allg. Chem.* **1957**, *291*, 12–50.
16. Fehér, F.; Wilucki, I.V.; Dost, G. Beiträge zur Kenntnis des Wasserstoffperoxyds und seiner Derivate, VII. Mittel.: Über die Kristallstruktur des Lithiumperoxyds, Li₂O₂. *Chem. Ber.* **1953**, *86*, 1429–1437. (In German)
17. Cota, L.G.; de la Mora, P. On the structure of lithium peroxide, Li₂O₂. *Acta Cryst.* **2005**, *B61*, 133–136.
18. Seriani, N. Ab initio thermodynamics of lithium oxides: From bulk phases to nanoparticles. *Nanotechnology* **2009**, *20*, 445703.
19. Mo, Y.; Ong, S.P.; Ceder, G. First-principles study of the oxygen evolution reaction of lithium peroxide in the lithium-air battery. *Phys. Rev. B* **2011**, *84*, 205446.
20. Radin, M.D.; Rodriguez, J.F.; Tian, F.; Siegel, D.J. Lithium peroxide surfaces are metallic, while lithium oxide surfaces are not. *J. Am. Chem. Soc.* **2012**, *134*, 1093–1103.
21. Radin, M.D.; Siegel, D.J. Charge transport in lithium peroxide: Relevance for rechargeable metal-air batteries. *Energy Environ. Sci.* **2013**, *6*, 2370–2379.
22. Lau, K.; Curtiss, L.; Chan, M.Y.; Greeley, J. Atomistic and first principles: Computational Studies of LiO₂ Batteries. In *The Lithium Air Battery*; Imanishi, N., Luntz, A.C., Bruce, P., Eds.; Springer: New York, NY, USA, 2014; pp. 159–177.
23. Lau, K.C.; Curtiss, L.A.; Greeley, J. Density functional investigation of the thermodynamic stability of lithium oxide bulk crystalline structures as a function of oxygen pressure. *J. Phys. Chem. C* **2011**, *115*, 23625–23633.
24. Chan, M.K.Y.; Shirley, E.L.; Karan, N.K.; Balasubramanian, M.; Ren, Y.; Greeley, J.P.; Fister, T.T. Structure of lithium peroxide. *J. Phys. Chem. Lett.* **2011**, *2*, 2483–2486.
25. Hummelshøj, J.S.; Blomqvist, J.; Datta, S.; Vegge, T.; Rossmeisl, J.; Thygesen, K.S.; Luntz, A.C.; Jacobsen, K.W.; Nørskov, J.K. Communications: Elementary oxygen electrode reactions in the aprotic Li-air battery. *J. Chem. Phys.* **2010**, *132*, 071101.
26. Garcia-Lastra, J.M.; Bass, J.D.; Thygesen, K.S. Communication: Strong excitonic and vibronic effects determine the optical properties of Li₂O₂. *J. Chem. Phys.* **2011**, *135*, 121101.
27. Kang, J.; Jung, Y.S.; Wei, S.H.; Dillon, A.C. Implications of the formation of small polarons in Li₂O₂ for Li-air batteries. *Phys. Rev. B* **2012**, *85*, 035210.
28. Nandy, A.K.; Mahadevan, P.; Sarma, D.D. K₂O₂: The most stable oxide of K. *Phys. Rev. B* **2011**, *84*, 035116.
29. Novis, S.W. Method for Preparing Lithium Peroxide. U.S. Patent 3446588, 27 May 1969.

30. Yang, J.; Zhai, D.; Wang, H.H.; Lau, K.C.; Schlueter, J.A.; Du, P.; Myers, D.J.; Sun, Y.K.; Curtiss, L.A.; Amine, K. Evidence for lithium superoxide-like species in the discharge product of a Li-O₂ battery. *Phys. Chem. Chem. Phys.* **2013**, *15*, 3764–3771.
31. Zhai, D.; Wang, H.H.; Yang, J.; Lau, K.C.; Li, K.; Amine, K.; Curtiss, L.A. Disproportionation in Li-O₂ batteries based on a large surface area carbon cathode. *J. Am. Chem. Soc.* **2013**, *135*, 15364–15372.
32. Zhai, D.; Wang, H.H.; Lau, K.C.; Gao, J.; Redfern, P.C.; Kang, F.; Li, B.; Indacochea, E.; Das, U.; Sun, H.H.; *et al.* Raman evidence for late stage disproportionation in a Li-O₂ battery. *J. Phys. Chem. Lett.* **2014**, *5*, 2705–2710.
33. Eysel, H.H.; Thym, S. RAMAN spectra of peroxides. *Z. Anorg. Allg. Chem.* **1975**, *411*, 97–102.
34. De Waal, D.; Range, K.J.; Königstein, M.; Kiefer, W. Raman spectra of the barium oxide peroxide and strontium oxide peroxide series. *J. Raman Spectrosc.* **1998**, *29*, 109–113.
35. Zhao, X.; Vanderbilt, D. First-principles study of structural, vibrational, and lattice dielectric properties of hafnium oxide. *Phys. Rev. B* **2002**, *65*, 233106.
36. Beuneu, F.; Vajda, P.; Jaskierowicz, G.; Lafleurielle, M. Formation of two kinds of nonspherical lithium colloids in electron-irradiated Li₂O single crystals. *Phys. Rev. B* **1997**, *55*, 11263.
37. Gonze, X.; Lee, C. Dynamical matrices, Born effective charges, dielectric permittivity tensors, and interatomic force constants from density-functional perturbation theory. *Phys. Rev. B* **1997**, *55*, 10355.
38. Ghosez, P.; Michenaud, J.P.; Gonze, X. Dynamical atomic charges: The case of ABO₃ compounds. *Phys. Rev. B* **1998**, *58*, 6224.
39. Tian, F.; Radin, M.D.; Siegel, D.J. Enhanced charge transport in amorphous Li₂O₂. *Chem. Mater.* **2014**, *26*, 2952–2959.
40. Lau, K.C.; Lu, J.; Luo, X.; Curtiss, L.A.; Amine, K. Implications of the unpaired spins in Li-O₂ battery chemistry and electrochemistry: A minireview. *ChemPlusChem* **2014**, doi:10.1002/cplu.201402053.
41. Zhao, Y.; Ban, C.; Kang, J.; Santhanagopalan, S.; Kim, G.H.; Wei, S.H.; Dillon, A.C. P-type doping of lithium peroxide with carbon sheets. *Appl. Phys. Lett.* **2012**, *101*, 023903.
42. Ong, S.P.; Mo, Y.; Ceder, G. Low hole polaron migration barrier in lithium peroxide. *Phys. Rev. B* **2012**, *85*, 081105.
43. Garcia-Lastra, J.M.; Myrdal, J.S.G.; Christensen, R.; Thygesen, K.S.; Vegge, T. DFT+U study of polaronic conduction in Li₂O₂ and Li₂CO₃: Implications for Li-Air batteries. *J. Phys. Chem. C* **2013**, *117*, 5568–5577.
44. Lu, J.; Jung, H.J.; Lau, K.C.; Zhang, Z.; Schlueter, J.A.; Du, P.; Assary, R.S.; Greeley, J.; Ferguson, G.A.; Wang, H.H.; *et al.* Magnetism in lithium-oxygen discharge product. *ChemSusChem* **2013**, *6*, 1196–1202.
45. Tang, W.; Sanville, E.; Henkelman, G. A grid-based bader analysis algorithm without lattice bias. *J. Phys. Condens. Matter* **2009**, *21*, 084204.
46. Kresse, G.; Furthmüller, J. Efficiency of ab-initio total energy calculations for metals and semiconductors using a plane-wave basis set. *Comput. Mater. Sci.* **1996**, *6*, 15–50.
47. Togo, A.; Oba, F.; Tanaka, I. First-principles calculations of the ferroelastic transition between rutile-type and CaCl₂-type SiO₂ at high pressures. *Phys. Rev. B* **2008**, *78*, 134106.